

On the Beam Filling Factors of Molecular Clouds

QING-ZENG YAN,¹ JI YANG,¹ YANG SU,¹ YAN SUN,¹ AND CHEN WANG¹

¹*Purple Mountain Observatory and Key Laboratory of Radio Astronomy,
Chinese Academy of Sciences, 10 Yuanhua Road, Qixia District, Nanjing 210033, People's Republic of China*

(Dated: December 13, 2021)

Submitted to ApJ

ABSTRACT

Imaging surveys of CO and other molecular transition lines are fundamental to measuring the large-scale distribution of molecular gas in the Milky Way. Due to finite angular resolution and sensitivity, however, observational effects are inevitable in the surveys, but few studies are available on the extent of uncertainties involved. The purpose of this work is to investigate the dependence of observations on angular resolution (beam sizes), sensitivity (noise levels), distances, and molecular tracers. To this end, we use high-quality CO images of a large-scale region ($25.8 < l < 49.7$ and $|b| < 5^\circ$) mapped by the Milky Way Imaging Scroll Painting (MWISP) survey as a benchmark to simulate observations with larger beam sizes and higher noise levels, deriving corresponding beam filling and sensitivity clip factors. The sensitivity clip factor is defined to be the completeness of observed flux. Taking the entire image as a whole object, we found that ^{12}CO has the largest beam filling and sensitivity clip factors and C^{18}O has the lowest. For molecular cloud samples extracted from images, the beam filling factor can be described by a characteristic size, $l_{1/4} = 0.762$ (in beam size), at which the beam filling factor is approximately 1/4. The sensitivity clip factor shows a similar relationship but is more correlated with the mean voxel signal-to-noise ratio of molecular clouds. This result may serve as a practical reference on beam filling and sensitivity clip factors in further analyses of the MWISP data and other observations.

Keywords: Molecular clouds (1072); Interstellar clouds (834); Interstellar molecules (849) ; Extragalactic astronomy(506); Astronomy data modeling(1859)

1. INTRODUCTION

Molecular clouds are a kind of neutral interstellar medium (ISM) (Heyer & Dame 2015), characterized with low temperatures (Mathis et al. 1983) and relatively high densities (Dame et al. 2001). In terms of morphology, molecular clouds are clumpy (Norman & Silk 1980) with fractal boundaries (Falgarone et al. 1991; Stutzki et al. 1998; Stanimirovic et al. 1999), and many show filamentary structures at large scale (Bally et al. 1987; Molinari et al. 2010; André et al. 2010). Having this particular kind of structure, the surface brightness temperature of molecular clouds is inhomogeneous (Burton et al. 1990), causing non-unity beam filling factors subjected to observations with finite beam sizes and sensitivities. However, beam filling factors are usually assumed to be unity in the calculation of physical properties, such as the excitation temperature, the optical depth, and the mass, which is inaccurate and may introduce systematic errors.

Observationally, the beam filling factor appears to be an item of diminishing the brightness temperature (e.g., Mangum & Shirley 2015). In the low temperature approximation, the specific form of the radiative equation is

$$T_{\text{mb}} = \eta (T_{\text{ex}} - T_{\text{bg}}) (1 - \exp(-\tau)), \quad (1)$$

where T_{mb} is the observed brightness temperature, η is the beam filling factor, T_{ex} is the excitation temperature, T_{bg} is the background temperature, and τ is the optical depth. However, in practical observations, T_{mb} is clipped due to the limited sensitivity, i.e., the brightness temperature below sensitivity is clipped to be zero in the observational data. We refer to this sensitivity effect (flux completeness) as the sensitivity clip factor, ξ . Obviously, the observed brightness temperature of molecular clouds is an interplay of sensitivity and angular resolution.

ξ , the sensitivity clip factor, is defined as the ratio of the observed flux and the total flux. The total flux corresponds to the flux at perfect sensitivity, and can be estimated by extrapolation from the observed flux at different sensitivity levels. The observed flux, however, corresponds to the flux at finite sensitivity.

Geometrically, the beam filling factor can also be defined by

$$\eta \approx \frac{\Omega_{\text{s}}}{\Omega_{\text{A}}}, \quad (2)$$

where Ω_{s} is solid angle of objects within the antenna beam and Ω_{A} is the beam solid angle, respectively. Apparently, for an object with a uniform brightness temperature across Ω_{A} , Ω_{s} equals Ω_{A} , i.e., $\eta = 1$, otherwise $\eta < 1$.

Beam filling factor effects are particularly severe in extragalactic observations. For example, [Rosolowsky & Leroy \(2006\)](#) studied the bias of Giant molecular cloud (GMC) properties caused by limited resolutions (spatial and spectral) and sensitivities toward galaxies in the Local Group. They found the measurement bias could be more than 40% and recommended a quadratic extrapolation to correct the flux of molecular clouds. [Sun et al. \(2018\)](#) studied molecular cloud properties in 15 nearby galaxies with spatial resolution of 45-120 pc, and given the size of molecular cloud complexes (~ 100 pc; [Motte et al. 2018](#)), the beam filling factors of extragalactic GMCs under Atacama Large Millimeter Array (ALMA) observations may be significantly less than unity. They concluded that the beam filling factor may cause the virial parameter (α_{vir}) to be overestimated, due to the underestimation of molecular cloud mass. [Dassat-Terrier et al. \(2019\)](#) derived a surface beam filling factor of ~ 0.05 for ^{12}CO cloud clumps toward M31 (with 11-pc resolution), and in the central region, the beam filling factor of dense gas is less than 0.02 with a resolution of about 100 pc ([Melchior & Combes 2016](#)). For some studies, such as metallicity gradients ([Acharyya et al. 2020](#)) and radiative transfer analyses subjected to sub-beam structures ([Leroy et al. 2017](#)), the beam size effect is pivotal.

Observations of molecular clouds in the Milky Way are also not free of beam dilution and sensitivity clip effects, particularly for molecular clouds with small angular sizes. Due to the inhomogeneity, beam smoothing diminishes the peak and edge brightness temperatures, and when observed with finite sensitivities and spatial resolutions, both the flux and the brightness temperature are underestimated. For instance, [Yan et al. \(2020\)](#) found a completeness of 80% for the observed flux of local molecular clouds in the first Galactic quadrant. This completeness is expected to be lower for molecular clouds in distant spiral arms. In addition to the flux completeness, [Gong et al. \(2018\)](#) found with numerical simulations that the X_{CO} factor would increase by a factor of 2 if the beam size increases by a factor of 100 (from 1 to 100 pc). In addition to molecular clouds, the beam filling factor of H I gas is also less than unity. For instance, [Heiles & Troland \(2003\)](#) derived a value of ~ 0.5 for the warm H I gas. The beam filling factor can be the largest error source for analyses of small objects, for example, in the study of molecular outflows ([Flower et al. 2010](#)).

Conventionally, η can be estimated in two ways. The first method uses Equation 1 and an optically thick spectral line with an assumed excitation temperature, but this is inaccurate due to unknown optical depths and guessed excitation temperatures. The other approach is based on the assumption of Gaussian source distribution ([Pineda et al. 2008](#)). Under this assumption, the beam filling factor is estimated to be $\Theta_{\text{s}}^2 / (\Theta_{\text{s}}^2 + \Theta_{\text{b}}^2)$, where Θ_{b} and Θ_{s} are the beam size and full width at half maximum (FWHM) of the source, respectively. This is a good approximation for stars and dense cores, but for molecular clouds, whose surface brightness temperature distributions are usually none-Gaussian, the beam filling factor may not follow this convolution approach.

In this paper, we use images of three CO isotopologue lines in the first Galactic quadrant ($25^{\circ}8 < l < 49^{\circ}7$, $|b| < 5^{\circ}$, and $-79 < V_{\text{LSR}} < 139 \text{ km s}^{-1}$) to study observational effects on spectroscopic survey data of molecular clouds, including the beam filling and sensitivity clip factors. This region has been mapped by the Milky Way Imaging Scroll Painting (MWISP) CO survey ([Su et al. 2019](#)) with high sensitivity ($\sim 0.5 \text{ K}$ for ^{12}CO) and medium angular resolution (about $50''$). The high dynamical range of the MWISP survey in scale makes this region a superb data set for studying the beam filling factor. The entire data set is roughly divided into four spiral arms based on their radial velocities, and examinations of beam filling factors are subsequently performed on those arm segments.

This paper is organized as follows. The next section (Section 2) describes the CO data, cloud identification methods, and the beam filling and sensitivity clip factor models. Section 3 presents results of beam filling and sensitivity clip

Table 1. Observation parameters of three CO isotopologue lines of the MWISP survey.

Tracer	Rest frequency	Effective critical density ^a	HPBW	T_{sys}	δv	rms noise
	(GHz)	(10^3 cm^{-3})	($''$)	(K)	(km s^{-1})	(K)
$^{12}\text{CO } (J = 1 \rightarrow 0)$	115.27	~ 0.06	49	220-300	0.158	~ 0.49
$^{13}\text{CO } (J = 1 \rightarrow 0)$	110.20	~ 6	52	140-190	0.166	~ 0.23
$\text{C}^{18}\text{O } (J = 1 \rightarrow 0)$	109.78	~ 18	52	140-190	0.167	~ 0.23

^aThe effective critical density takes account of radiative line trapping (Yan et al. 2019).

factors, including collective and individual molecular clouds. Discussions are presented in Section 4, and we summarize the conclusions in Section 5.

2. DATA AND METHODS

2.1. CO data

We select a region in the first Galactic quadrant ($25^\circ.8 < l < 49^\circ.7$, $|b| < 5^\circ$, and $-79 < V_{\text{LSR}} < 139 \text{ km s}^{-1}$) to study the beam filling and sensitivity clip factors, and this region has been uniformly mapped by the MWISP¹ CO survey (Su et al. 2019). Observations were performed with the Purple Mountain Observatory (PMO) 13.7-m millimeter telescope, containing three CO isotopologue line maps, $^{12}\text{CO } (J = 1 \rightarrow 0)$, $^{13}\text{CO } (J = 1 \rightarrow 0)$, and $\text{C}^{18}\text{O } (J = 1 \rightarrow 0)$, which were all used in this work.

The angular resolution of these line maps are approximately $49''$, $52''$, and $52''$, and the velocity resolutions are 0.158 , 0.166 , and 0.167 km s^{-1} , respectively. The pixel size of the regridded map is $30''$. The rms noise of ^{12}CO is about 0.49 K , $\sim 0.23 \text{ K}$ for ^{13}CO and C^{18}O . See Table 1 for a summary of the observation parameters.

In order to investigate the beam filling and sensitivity clip effects at different distance layers, we roughly split each of the three isotopologue data cubes into four arm segments (Reid et al. 2016) along the V_{LSR} axis: (1) the Local arm (-6 to 30 km s^{-1}); (2) the Sagittarius arm (30 to 70 km s^{-1}); (3) the Scutum arm (70 to 139 km s^{-1}); (4) the Outer and Outer Scutum-Centaurus arm (-79 to -6 km s^{-1}). Based on kinematic distances (A5 model in Reid et al. 2014), distances of the four spiral arms are approximately 1 , 3 , 6 , and 15 kpc , respectively. The Perseus arm is largely overlapped with the Local arm in V_{LSR} space, so we ignored the Perseus arm. Consequently, three CO lines collectively yield 12 data cubes.

2.2. Molecular cloud samples

In order to investigate the beam filling and sensitivity clip factors of different molecular cloud species, we use the DBSCAN² algorithm to draw samples from the position-position-velocity (PPV) cubes (Yan et al. 2020). DBSCAN ignores internal structures of molecular clouds and identifies independent structures in PPV space, sufficing for the beam filling factor studies.

In PPV space, DBSCAN has two parameters, MinPts and the connectivity. The connectivity (three types in PPV space) defines the neighborhood of each voxel, i.e., whether two voxels are connected. For a given voxel, if the number of its neighboring voxels (including itself) is $\geq \text{MinPts}$, it is a core point, and connecting core points and their neighbors define a molecular cloud. As discussed in Yan et al. (2020), for small MinPts values, the three connectivity types provide similar cloud samples, so we simply use connectivity 1 and MinPts 4. The minimum cutoff of the data cube is 2σ ($\sim 1 \text{ K}$ for ^{12}CO and $\sim 0.5 \text{ K}$ for ^{13}CO and C^{18}O), and in practice, the rms noise calculation is accurate to each spectrum.

We applied the post selection criteria to remove small DBSCAN clusters that are likely to be noise (Yan et al. 2020). The post selection criteria contain four conditions: (1) the voxel number is ≥ 16 ; (2) the peak brightness temperature is $\geq 5\sigma$; (3) the projection area contains a beam (a compact 2×2 region equivalent to $60'' \times 60''$); (4) the velocity channel number is ≥ 3 .

¹ <http://www.radioast.nsd.cn/mwisp.php>

² <https://scikit-learn.org/stable/modules/generated/sklearn.cluster.DBSCAN.html>

2.3. Beam filling and sensitivity clip factors

The beam filling and sensitivity clip factors have different applications. The beam filling factor is used to correct T_{mb} to obtain accurate excitation temperatures and optical depths, while the sensitivity clip factor is used to correct the observed flux, which is more related to, e.g., the mass of molecular clouds. η strongly depends on the beam size, and we refer to η as the value at the angular resolution of the data. For a single pixel, ξ is either unity or zero, but for an image or a molecular cloud, the observed flux above cutoffs is the inverse cumulative distribution function of CO brightness temperatures, and ξ describes the observed fraction of the flux.

η and ξ can be estimated in two approaches: (1) based on the entire image and (2) based on molecular cloud samples. In the first image-based case, the whole data cube is taken as a single molecular cloud, while in the second sample-based case, the estimation is performed for each molecular cloud sample identified with the method described in Section 2.2.

The variation of η and ξ is modeled with extrapolation functions. Without a physically motivated theory at hand, we use an empirical function. However, the extrapolation function should be simple and versatile, applicable to both image-based and sample-based cases.

In order to model η and ξ , we produce two data sets based on the MWISP CO data. The first data set simulates a series of observations at different beam sizes and is used to estimate η . For the convenience of calculation, we keep the pixel size constant in smoothing. The second data set, however, resembles observations with the same beam size but different sensitivity clips and is used to estimate ξ .

2.3.1. Beam filling factors

For an isolated Gaussian source, the variation of its peak brightness temperature is proportional to the beam filling factor, but for molecular clouds, which are irregular and have non-uniform brightness distribution, we can take each voxel in a data cube as a Gaussian peak. In this case, the beam filling factor can be examined voxel by voxel based on intensity, but the signal-to-noise ratio (SNR) of a single voxel is low, causing large errors in curve fitting, particularly for extended weak components of molecular clouds. In order to obtain high SNRs, we take each molecular cloud as an object and use the mean T_{mb} to derive an average beam filling factor.

For specific observation data, the rms noise and the angular resolution are coupled. Smoothing operations decrease both T_{mb} and the rms noise, and in the estimation of η , voxels are need to be above the sensitivity level in all simulated observations. In other words, voxels that are below the sensitivity level in a smoothing case are discarded. The sensitivity level we used is 2σ , consistent with DBSCAN parameters. However, σ is different between smoothing cases.

The procedure of obtaining η contains three main steps: (1) identifying molecular clouds, (2) smoothing data cubes, and (3) modeling η . The first step applies the procedure of producing molecular cloud samples (see Section 2.2) on raw CO data.

In the second step, data cubes are smoothed to simulate observations with larger beam sizes. The smoothing operation is performed with the `spectral-cube` package³ in Python language. The beam size varies by factors from 1.5 to 10 with an interval of 0.5, giving 18 smoothing cases in total. For the convenience of comparing, we keep the voxel size unchanged. The rms noise is calculated with the Outer arm cubes, which contain the largest amount of noise voxels, and we use the rms of negative values in the spectra as a proxy of the rms noise.

In the third step, we estimate η based on the variation of mean T_{mb} with respect to the beam size. The mean T_{mb} is obtained by averaging brightness temperatures over voxels that are above the sensitivity clip levels in all smoothing cases. η is obtained through extrapolation, and taking the mean T_{mb} at the zero-beam point as observations with infinite angular resolutions ($\eta = 1$), the fraction of T_{mb} at a specific beam size is the corresponding beam filling factor. For MWISP molecular clouds, we use the fraction at the MWISP beam size as their beam filling factors.

We found that the mean T_{mb} roughly contains two components, a linear part and an exponential part, which can be well described by a four-parameter function:

$$T(\Theta) = a \exp(-b\Theta) - c\Theta + d, \quad (3)$$

where, Θ represents the beam size, y is the corresponding observed flux, and a , b , c , and d are four parameters to be determined. Equation 3 is approximately linear when b is small and is also able to fit flux variations that decrease

³ <https://spectral-cube.readthedocs.io/en/latest/index.html>

fast (with large b values). The superiority of this function over polynomials is that the meaning of Equation 3 is more clear, and Equation 3 is a monotonic function, which satisfies the intuition that flux decreases with larger beam sizes.

We use Equation 3 to extrapolate the value of the mean T_{mb} to zero. The variation of the mean T_{mb} is fitted with `curve_fit` in the Python package SciPy with flux errors considered. The error of the mean T_{mb} is estimated with $\sqrt{\sum_i \sigma_i^2 / N}$, where N is the voxel number and σ_i is the rms noise of each voxel. σ_i decreases with beam sizes but N is constant. Specifically, the beam filling factor is estimated with Equation 3 using

$$\eta = \frac{T(\Theta_{\text{MWISP}})}{T(0)}, \quad (4)$$

where $T(\Theta_{\text{MWISP}})$ and $T(0)$ is the mean T_{mb} at the MWISP beam size and at zero-beam size, respectively. Errors of $T(\Theta_{\text{MWISP}})$ and $T(0)$ are obtained with first derivatives of T at Θ_{MWISP} and 0, respectively, together with the covariance of a , b , and c , and the error of η is subsequently estimated with propagation of errors.

2.3.2. Sensitivity clip factors

In this section, we present the method of deriving ξ . We use the cutoff as a proxy of the sensitivity clip levels, simulating observations at different sensitivities but with the same angular resolution. In this context, the flux above the cutoff is the inverse of the cumulative distribution function of the brightness temperature.

The procedure of modeling ξ is similar to that of η . By definition, ξ approaches unity as the sensitivity goes infinity, and ξ corresponds to the completeness of the flux at a specific sensitivity level. The cutoffs range from 2σ to 20σ with an interval of 0.2σ . ξ is the fraction of observed flux at 2σ with respect to the zeroth flux obtained with extrapolation.

Equation 3 cannot model the flux variation with respect to the sensitivity (the brightness temperature cutoff). Instead, we found that the quadratic equation suggested by Rosolowsky & Leroy (2006) is more appropriate. However, toward high cutoffs, the observed flux of molecular clouds usually decreases rapidly to zero, so we use a sigmoid term that contains the Gaussian CDF to model this zero tail.

specifically, the observed flux (f) above the cutoff (x) is approximately

$$\begin{cases} \text{erf}(z) = \frac{2}{\sqrt{\pi}} \int_0^z \exp(-t^2) dt, \\ F(x) = \frac{1}{2} \left(1 + \text{erf} \left(\frac{x-\mu}{\sqrt{2}\delta} \right) \right), \\ f(x) = (a(x-b)^2 + c) (1 - F(x)), \end{cases} \quad (5)$$

where $F(x)$ is the cumulative distribution function (CDF) of Gaussian distribution $\mathcal{N}(\mu, \delta)$, x is in units of rms noise (σ), and $f(x)$ is the observed flux above x . Due to the sigmoid item that contains the Gaussian CDF, $f(x)$ is forced to approximate 0 for large x values. In total, Equation 5 contains 5 parameters: a , b , c , μ , and δ , and for a normal fitting, a , b , and δ should be positive. ξ is estimated subsequently with

$$\xi = \frac{f(\sigma_{\text{cut}})}{f(0)}, \quad (6)$$

where σ_{cut} is the T_{mb} cutoff (in the unit of rms noise) of molecular clouds.

3. RESULTS

3.1. Image-based beam filling factors

In this section, we demonstrate the results of imaged-based beam filling factors. Image-based beam filling factors are calculated by taking the whole data cube as a single molecular cloud. The observed mean T_{mb} toward four spiral arm segments is listed in Table 2, including all smoothing cases. No C^{18}O emission is detected toward the Outer arm, i.e., the beam filling factor of C^{18}O in the Outer arm is approximately zero.

As examples, we display variations of the mean T_{mb} and the image-base η of local molecular clouds in Figure 1. The relative errors are small, about 1×10^{-4} . The patterns of the mean T_{mb} variations are similar for three CO lines, and Equation 3 fits the variation of the mean T_{mb} well, except a slight deviation for the mean T_{mb} of the raw data. This systematic shift of the mean T_{mb} between raw and smoothing data is discussed in Section 4.1. As expected, ^{12}CO has the highest η , while C^{18}O has the lowest.

Table 3 summarizes η of three CO lines in four spiral arm segments. η of ^{12}CO and ^{13}CO in the Local, Sagittarius, and Scutum arm are approximately unity, while η of C^{18}O are significantly lower. In the Outer arm, however, both ^{12}CO and ^{13}CO have low beam filling factors.

Table 2. Variation of the mean T_{mb} with respect to beam sizes for molecular clouds in four Galactic arm segments.

		Beam sizes																		
Arm	Line	1	1.5	2	2.5	3	3.5	4	4.5	5	5.5	6	6.5	7	7.5	8	8.5	9	9.5	10
		(K)																		
Local	^{12}CO	2.55	2.46	2.42	2.39	2.37	2.35	2.33	2.31	2.29	2.28	2.26	2.25	2.23	2.22	2.21	2.19	2.18	2.17	2.16
	^{13}CO	1.22	1.15	1.12	1.10	1.08	1.06	1.05	1.03	1.02	1.01	0.996	0.985	0.975	0.965	0.955	0.946	0.937	0.928	0.920
	C^{18}O	0.950	0.836	0.792	0.762	0.736	0.713	0.692	0.672	0.654	0.637	0.622	0.607	0.593	0.580	0.567	0.556	0.544	0.534	0.524
Sagittarius	^{12}CO	2.72	2.61	2.56	2.52	2.48	2.45	2.42	2.40	2.37	2.35	2.32	2.30	2.28	2.26	2.24	2.23	2.21	2.19	2.18
	^{13}CO	1.22	1.12	1.08	1.04	1.01	0.986	0.961	0.938	0.917	0.897	0.878	0.861	0.844	0.829	0.814	0.800	0.787	0.774	0.762
	C^{18}O	0.867	0.724	0.657	0.608	0.566	0.529	0.497	0.468	0.442	0.419	0.398	0.378	0.361	0.344	0.329	0.316	0.303	0.291	0.280
Scutum	^{12}CO	3.06	2.96	2.92	2.88	2.85	2.82	2.80	2.77	2.75	2.73	2.71	2.69	2.67	2.65	2.63	2.62	2.60	2.59	2.57
	^{13}CO	1.29	1.20	1.16	1.12	1.09	1.06	1.04	1.02	0.994	0.974	0.955	0.938	0.921	0.906	0.892	0.878	0.865	0.852	0.840
	C^{18}O	0.914	0.765	0.694	0.642	0.598	0.560	0.527	0.497	0.471	0.448	0.426	0.407	0.390	0.374	0.359	0.346	0.333	0.322	0.311
Outer	^{12}CO	1.93	1.68	1.53	1.41	1.30	1.21	1.13	1.06	0.998	0.942	0.891	0.844	0.802	0.764	0.729	0.696	0.666	0.638	0.613
	^{13}CO	0.924	0.753	0.660	0.590	0.533	0.486	0.446	0.412	0.382	0.356	0.332	0.312	0.293	0.276	0.261	0.247	0.234	0.223	0.212
	C^{18}O	0.000	0.000	0.000	0.000	0.000	0.000	0.000	0.000	0.000	0.000	0.000	0.000	0.000	0.000	0.000	0.000	0.000	0.000	0.000

NOTE—The beam size is in units of the MWISP beam, 49'' for ^{12}CO and 52'' for ^{13}CO and C^{18}O .**Table 3.** Image-based beam filling and sensitivity clip factors of the MWISP survey.

Arm	Line	V_{LSR}	η	ξ
(1)	(2)	(3)	(4)	(5)
Local	^{12}CO	[0, 30]	0.982 ± 0.000	0.766 ± 0.000
	^{13}CO		0.959 ± 0.000	0.676 ± 0.000
	C^{18}O		0.877 ± 0.001	0.450 ± 0.000
Sagittarius	^{12}CO	[30, 70]	0.980 ± 0.000	0.788 ± 0.000
	^{13}CO		0.941 ± 0.000	0.644 ± 0.000
	C^{18}O		0.722 ± 0.001	0.458 ± 0.001
Scutum	^{12}CO	[70, 139]	0.987 ± 0.000	0.834 ± 0.000
	^{13}CO		0.956 ± 0.000	0.702 ± 0.000
	C^{18}O		0.713 ± 0.000	0.480 ± 0.000
Outer	^{12}CO	[-79, -6]	0.777 ± 0.000	0.540 ± 0.000
	^{13}CO		0.613 ± 0.001	0.412 ± 0.001
	C^{18}O		—	—

3.2. Sample-based beam filling factors

The procedure of deriving beam filling factors for individual molecular clouds is similar to that of image-based beam filling factors, and the only difference is that the mean T_{mb} for each molecular cloud is calculated over its own region. This region is determined with raw (unsmoothed) MWISP data using DBSCAN (down to 2σ), and voxels involved in the estimate of the mean T_{mb} are required to be above 2σ level in all smoothing cases.

The beam filling factor of each molecular cloud is estimated with Equation 3 based on the variation of mean T_{mb} with respect to the beam size. As examples, we show η of four ^{12}CO molecular clouds in the Local arm in Figure 2. Usually, molecular clouds whose mean T_{mb} decreases approximately linearly have high beam filling factors, while molecular clouds with exponentially decreasing mean T_{mb} have low beam filling factors.

We found that η is correlated with the angular size l of molecular clouds. The angular size is defined as an equivalent diameter derived with

$$l = \sqrt{\frac{4A}{\pi} - \Theta_{\text{MWISP}}^2}, \quad (7)$$

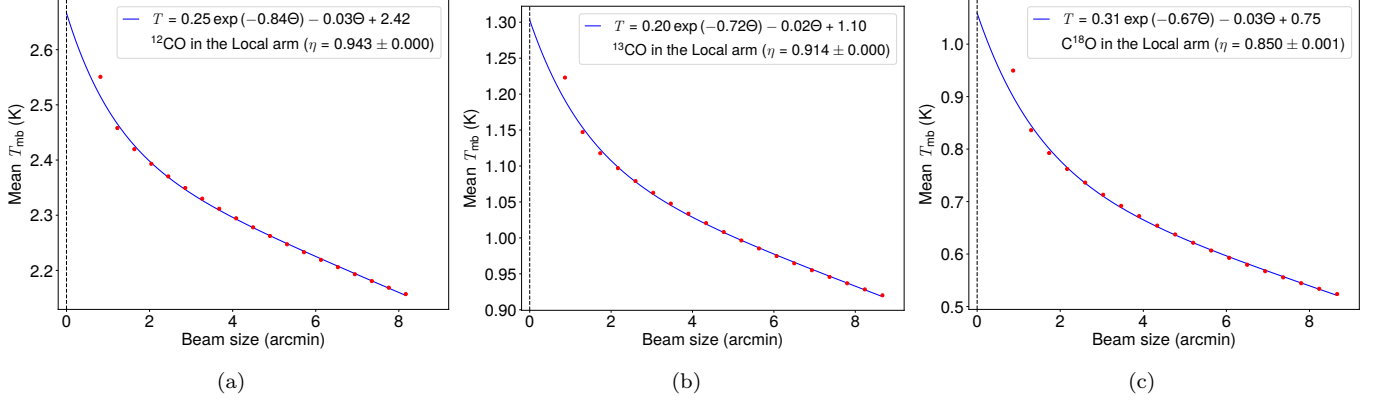


Figure 1. Variation of the mean T_{mb} against the beam size. Only local molecular clouds are displayed: (a) ^{12}CO , (b) ^{13}CO , and (c) C^{18}O . Red points are the observed flux for each smoothing case with different beam sizes, and the error bar is smaller than the marker size. The blue lines are fitted with red points using Equation 3.

where A is the angular area and Θ_{MWISP} is the beam size of the MWISP survey. Figure 3 demonstrates the η variation of ^{12}CO clouds against their angular sizes. Evidently, compared with the radial velocity (the color code), which is usually used as a distance indicator, η is more related to the angular size. η is approximately unity for molecular clouds with large angular sizes ($\geq 10'$), but decrease sharply for small ones.

Given the large dispersion of η , we only look for a first-order approximation for the relationship between η and l . The function we used is

$$\eta = \eta_{\text{max}} \frac{l^2}{(l + l_{1/4})^2}, \quad (8)$$

where $l_{1/4}$ is the angular size corresponding to $\eta = 0.25\eta_{\text{max}}$. With this model, the range of η is from 0 ($l \rightarrow 0$) to η_{max} ($l \rightarrow \infty$), and compared with other models (see Section 4.2), Equation 8 yields a smaller rms residual and has a clear physical meaning. Theoretically, η_{max} should equal one, but η_{max} is slightly less than one in practice, possibly due to the error of simulated data. The right side of Equation 8 is a ratio of the angular area of molecular clouds to the observed angular area enlarged by the beam, consistent with the beam filling factor definition. Consequently, we use Equation 8 to model the relationship between η and l . η_{max} and $l_{1/4}$ is solved with `curve_fit` of the Python package `SciPy`, considering the error of η .

Results of ^{12}CO molecular clouds are described in Figure 3, and values of $l_{1/4}$ for three CO lines and four spiral arms are summarized in Table 4. Remarkably, values of η_{max} and $l_{1/4}$ is approximately equal for molecular clouds in all four arms, suggesting that molecular clouds with close angular sizes have approximately equal beam filling factors despite being at different distances.

Given the similarity of η_{max} and $l_{1/4}$ in four arm segments, we fit overall values with all molecular clouds. As demonstrated in Figure 4, the overall fitting gives values of $l_{1/4} = 0.762 \pm 0.001$ and $\eta_{\text{max}} = 0.922 \pm 0.000$, i.e., η is approximately

$$\eta = \frac{0.922l^2}{(l + 0.762)^2}, \quad (9)$$

where l is the angular size of molecular clouds in units of the beam size.

3.3. Image-based sensitivity clip factors

Similar to the beam filling factor, the sensitivity clip factor can also be estimated by taking all emission as a single object. Figure 5 displays results of ξ for local molecular clouds. As can be seen, Equation 5 fits the flux variation well, but show slight deviations around 2σ cutoff. This is because at 2σ , the observed flux may not be complete due to the insufficient SNR.

Table 3 lists results of all four arm segments. Clearly, among three CO lines, ^{12}CO has the highest ξ , while C^{18}O has the smallest ξ . As to arm segments, the Scutum and Outer arm has the highest and lowest ξ , respectively, while the rest two arms have medium ξ .

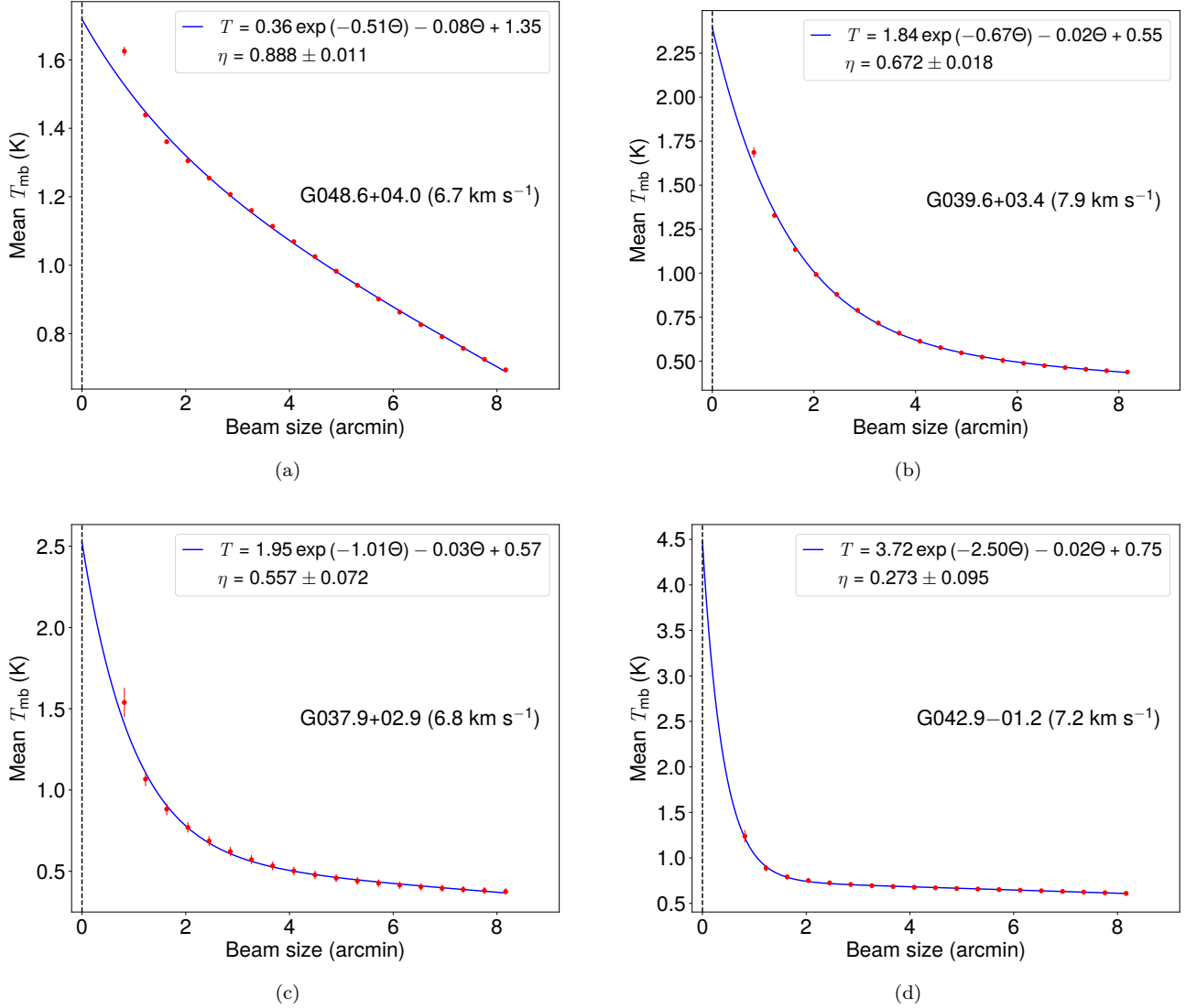


Figure 2. Same as Figure 1 but for four typical ^{12}CO clouds in the Local arm: (a) G048.6+04.0 at 6.7 km s^{-1} , (b) G039.6+03.4 at 7.9 km s^{-1} , (c) G037.9+02.9 at 6.8 km s^{-1} , and (d) G042.9-01.2 at 7.2 km s^{-1} .

3.4. Sample-based sensitivity clip factors

To make ξ consistent with η , the minimum cutoff of brightness temperature for individual molecular clouds is 2σ . In Figure 6, fitting results show that Equation 5 describes the flux variation well for individual molecular clouds.

We found that ξ are correlated with the mean voxel SNR of molecular clouds. This relationship is insensitive to molecular cloud tracers and distances, and can be described with Equation 8 but with a slight adjustment of zero points:

$$\xi = \frac{(x - x_0)^2}{(x - x_0 + x_{1/4})^2}, \quad (10)$$

where x_0 is the zero point and $x_{1/4}$ is the mean voxel SNR (with respect to x_0) at which $\xi = 1/4$.

Figure 7 demonstrates the relationship between the sensitivity clip factor and the mean voxel SNR, including molecular cloud samples of all four arm segments and three CO lines. The molecular cloud samples only contain normal fittings (25542 in total) of Equation 5, i.e., a , b , and δ are positive and $0 < \xi < 1$.

4. DISCUSSION

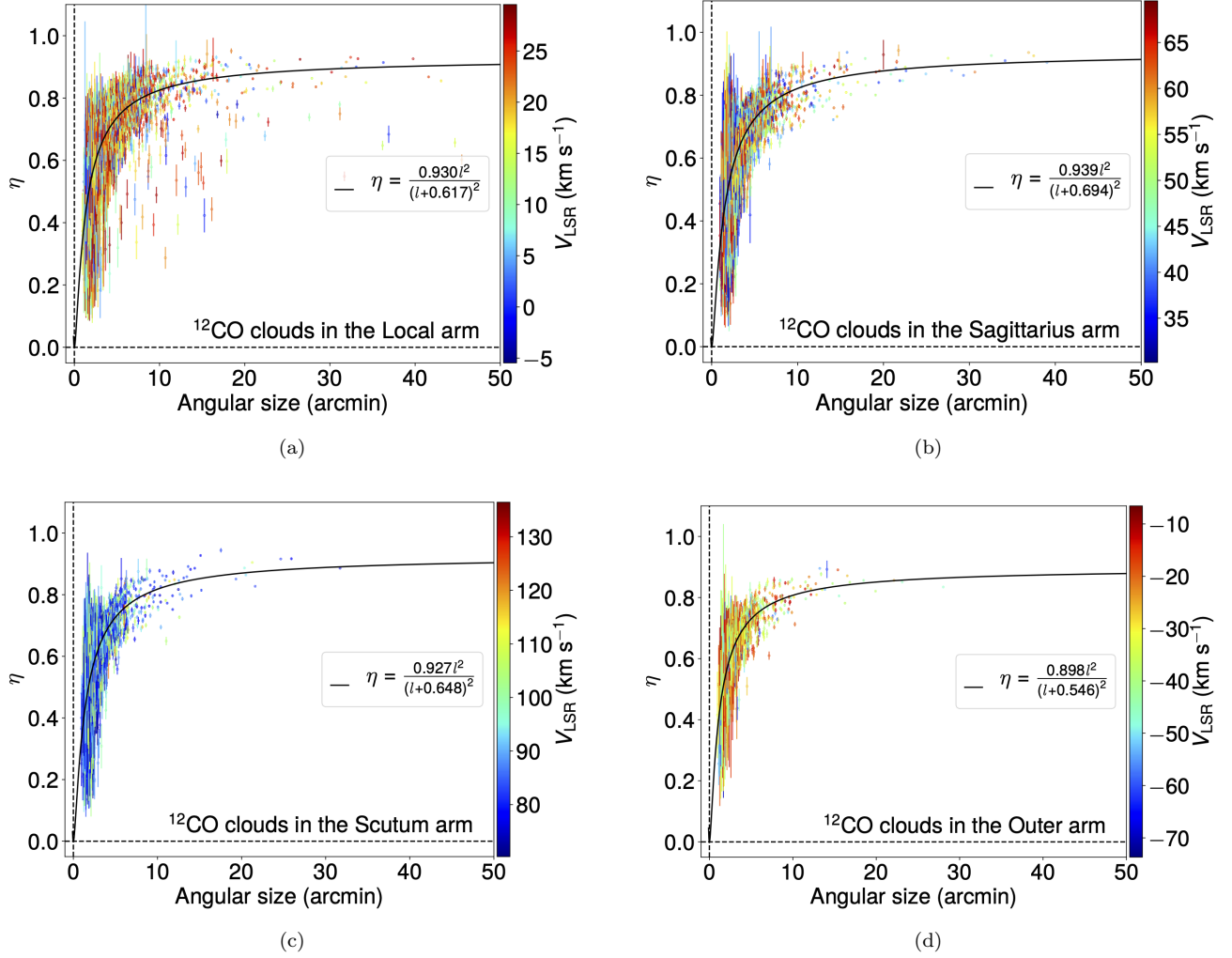


Figure 3. η of individual ^{12}CO clouds against their angular sizes in four spiral arm segments: (a) the Local arm, (b) the Sagittarius arm, (c) the Scutum arm, and (d) the Outer arm. The color code represents V_{LSR} , and see Equation 8 for the form of black solid lines.

4.1. Simulated data

In this work, we used simulated data instead of practical observations, which may cause systematic errors. The raw Data is clipped at a certain sensitivity level, and all smoothing cases are based on clipped images. Consequently, T_{mb} in simulated data is possibly systematically smaller (than practical observations) due to the clip effect of the raw data, particularly for voxels near the edge of molecular clouds.

This systematic shift of simulated T_{mb} is demonstrated in Figure 1. The mean T_{mb} of the raw data is slightly larger than the fitted value. This discrepancy can be examined with practical observations, which do not have this issue.

4.2. Beam filling factors and the angular size

Although we use Equation 8 to describe the relationship between the beam filling factor and the angular size, the choice of functions is not unique. We compared two additional function forms, and found that judging by the rms residual, Equation 8 outperforms the other two models. One of the two models uses the function

$$\eta = \frac{l^2}{(l^2 + a)}, \quad (11)$$

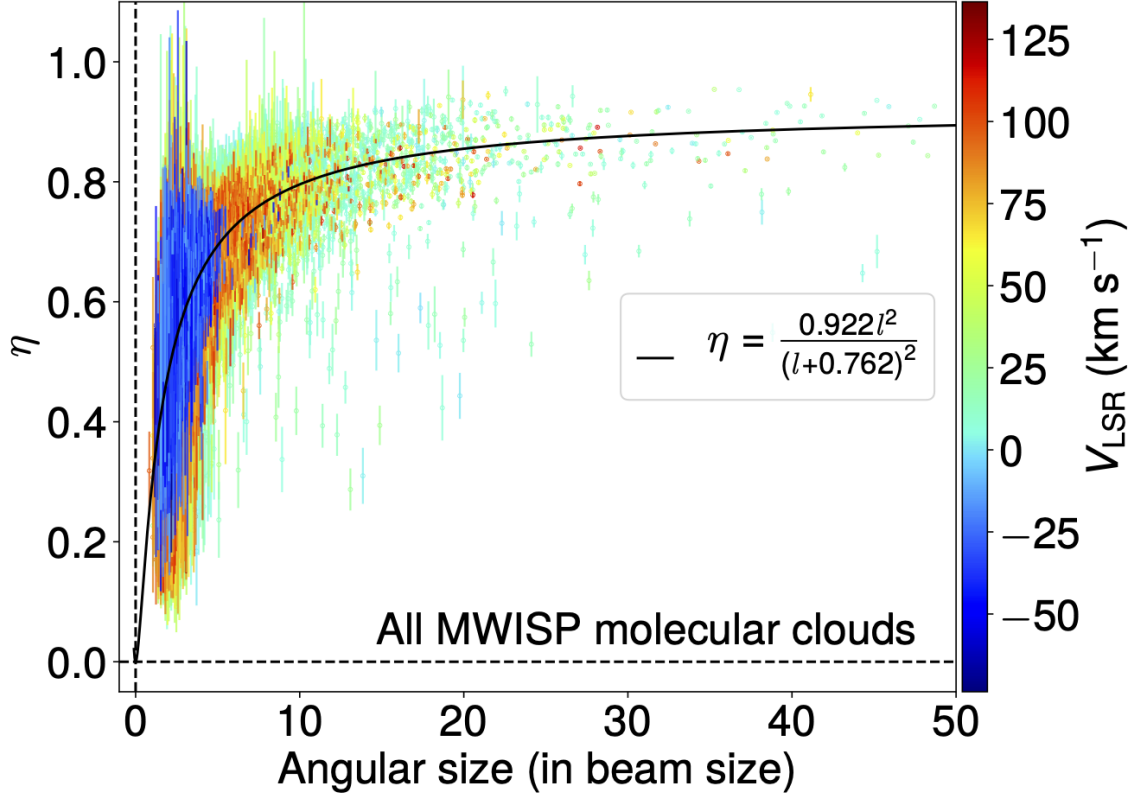


Figure 4. η - l relationship with all molecular cloud samples in four spiral arm segments, including ^{12}CO , ^{13}CO , and C^{18}O samples. See Equation 9 for the form of the black solid line.

Table 4. Beam filling and sensitivity clip factor relationships in the first Galactic quadrant based on the MWISP survey.

Arm	Line	$\eta = \eta_{\max} \frac{l^2}{(l+l_{1/4})^2}$		$\xi = \frac{(x-x_0)^2}{(x-x_0+x_{1/4})^2}$	
		η_{\max}	$l_{1/4}$	x_0	$x_{1/4}$
(1)	(2)	(3)	(4)	(5)	(6)
Local	^{12}CO	0.930 ± 0.000	0.617 ± 0.002	2.228 ± 0.001	0.455 ± 0.000
	^{13}CO	0.913 ± 0.000	0.593 ± 0.002	2.224 ± 0.001	0.456 ± 0.000
	C^{18}O	0.896 ± 0.001	0.474 ± 0.009	2.065 ± 0.005	0.523 ± 0.002
Sagittarius	^{12}CO	0.939 ± 0.000	0.694 ± 0.002	2.215 ± 0.001	0.460 ± 0.000
	^{13}CO	0.911 ± 0.000	0.628 ± 0.002	2.228 ± 0.001	0.463 ± 0.000
	C^{18}O	0.889 ± 0.002	0.542 ± 0.007	2.187 ± 0.004	0.472 ± 0.002
Scutum	^{12}CO	0.927 ± 0.001	0.648 ± 0.002	2.236 ± 0.001	0.448 ± 0.000
	^{13}CO	0.916 ± 0.001	0.657 ± 0.003	2.223 ± 0.002	0.451 ± 0.001
	C^{18}O	0.864 ± 0.001	0.503 ± 0.005	2.204 ± 0.004	0.468 ± 0.001
Outer	^{12}CO	0.898 ± 0.001	0.546 ± 0.004	2.248 ± 0.002	0.451 ± 0.001
	^{13}CO	0.864 ± 0.005	0.538 ± 0.017	2.138 ± 0.010	0.503 ± 0.004
	C^{18}O	—	—	—	—

NOTE— $l_{1/4}$ is in arcmin, while x_0 and $x_{1/4}$ are in rms noise.

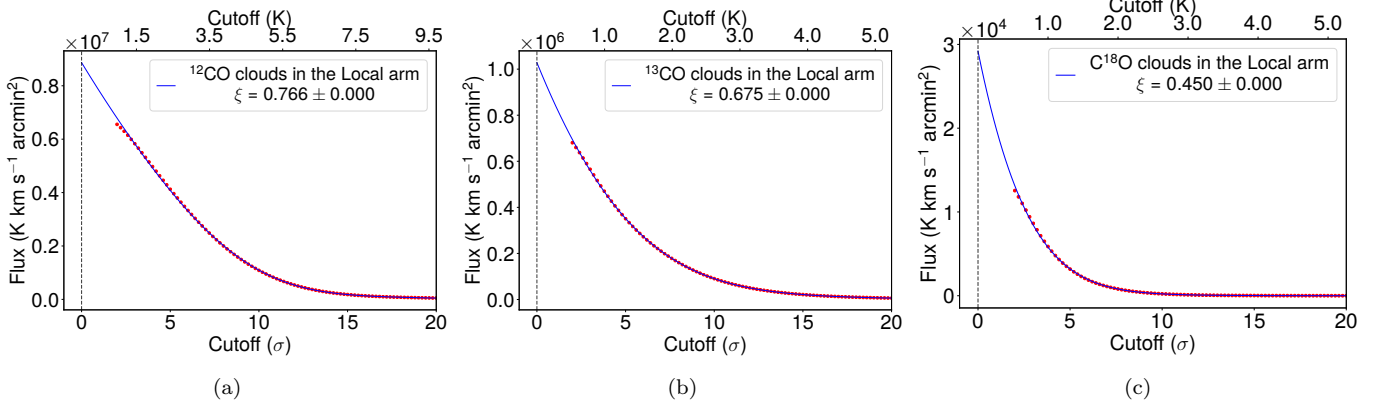


Figure 5. Fitting of image-based flux variation with respect to cutoffs in the Local arm: (a) ^{12}CO , (b) ^{13}CO , and (c) C^{18}O . Flux variations (blue lines) are modeled with Equation 5, and the corresponding ξ (see Equation 6 for the definition) is derived with the ratio of modeled flux values at 2σ to that at zero. The error bar is smaller than the marker size.

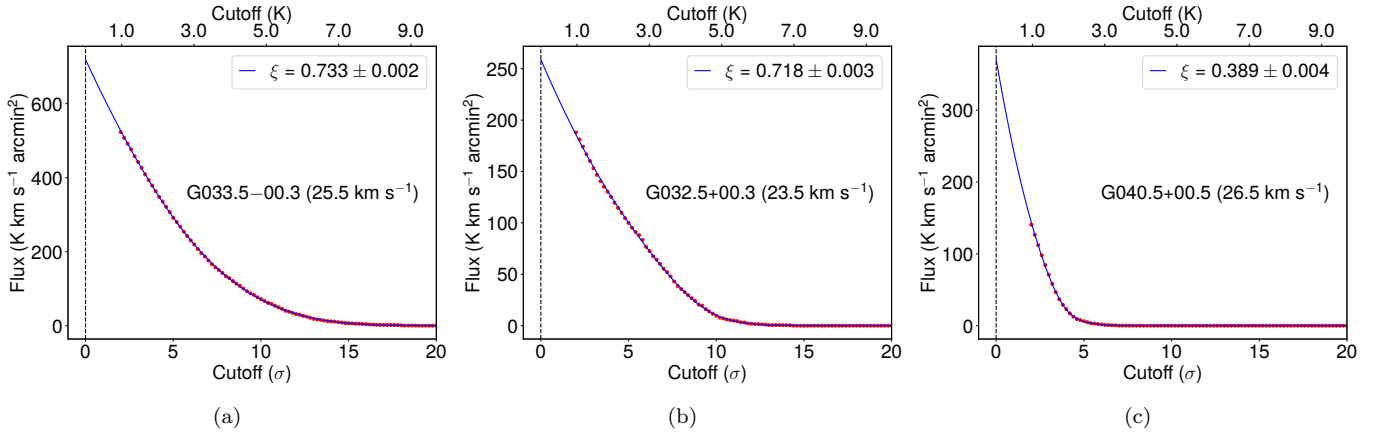


Figure 6. Same as Figure 5 but for three ^{12}CO clouds in the Local arm: (a) G033.5-00.3 at 25.5 km s^{-1} , (b) G032.5+00.3 at 23.5 km s^{-1} , and (c) G040.5+00.5 at 26.5 km s^{-1} .

where a is a parameter. Equation 11 resembles the convolution of Gaussian distributions (Pineda et al. 2008), while the third model has a form of

$$\eta = a(1 - \exp(-bl)), \quad (12)$$

where a and b are two parameters and l is the angular size of molecular clouds. In this case, $\eta \rightarrow 0$ as $l \rightarrow 0$, while $f \rightarrow a$ as $l \rightarrow \infty$, i.e., a is the maximum beam filling factor.

To test which model performs best, we split ^{12}CO molecular cloud samples in the Local arm into two categories: (1) the training set and (2) the validation data set. The training set is used to fit the model, while the validation data is used to verify the model. We examined two cases, having 20% and 30% validation data ratios, respectively, and the weighted rms residual (chi-square) of the validation data is used as an indicator of modeling qualities. As shown in Figure 8, Equation 8 possess the best performance.

4.3. Beam filling factors of molecular clouds

Beam filling factors of small molecular clouds are largely uncertain, while beam filling factors of large molecular clouds are well modeled. According to the relationship between the beam filling factor and the angular size of molecular clouds, beam filling factors are approximately unity for relatively large molecular clouds, and decrease fast toward small molecular clouds. Beam filling factors are less than 0.5 for molecular clouds with angular size less than ~ 2 beam sizes (after deconvolution), and given the large uncertainty, it could be even smaller.

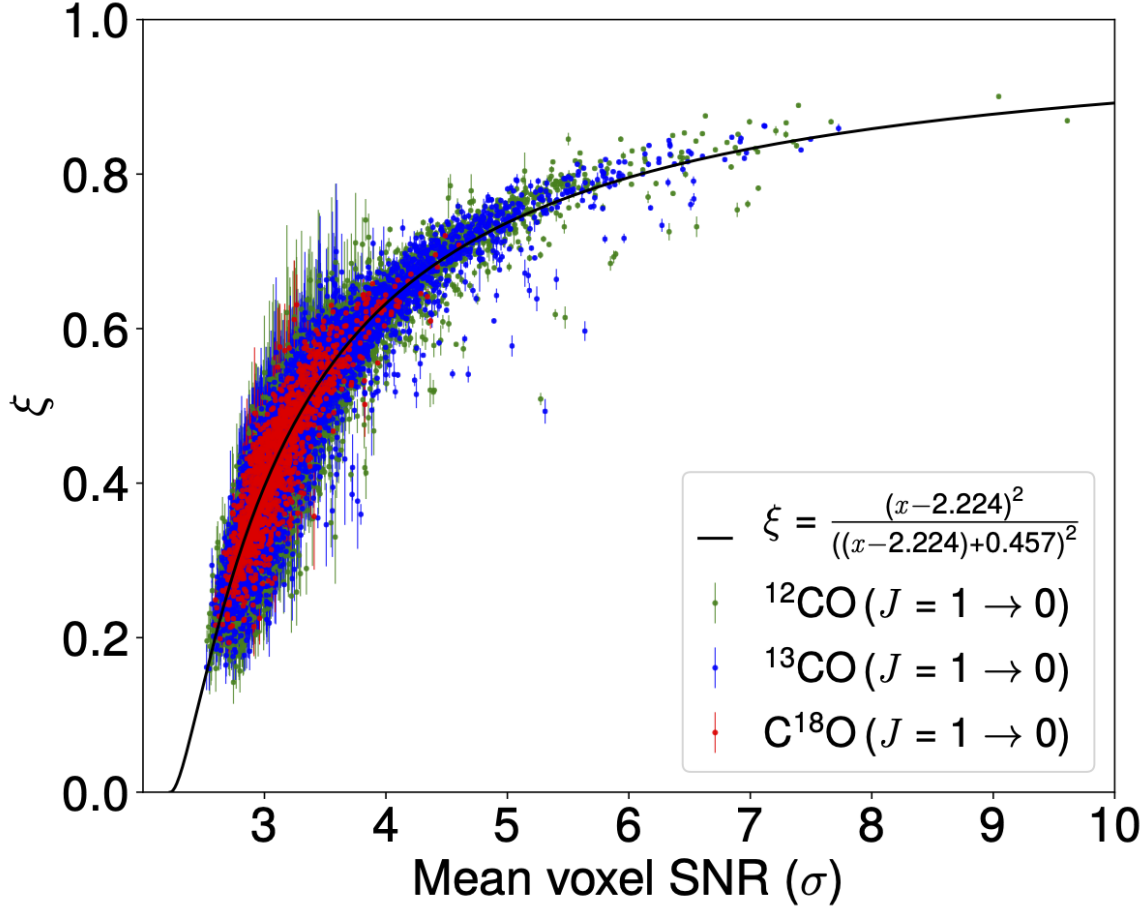


Figure 7. The relationship between the sample-based ξ and the mean voxel SNR. The mean voxel SNR is the mean SNR of all voxels in a molecular cloud. In the relationship fitting, all MWISP molecular clouds samples are used, including four arm segments and three CO isotopologue lines. For clarity purposes, only molecular clouds with relative errors less than 20% are displayed. The mean voxel SNR is in units of rms noise, and see Equation 5 for the black solid line.

Molecular cloud samples in this work is built with the DBSCAN detection scheme, but an alternative algorithm would yield different molecular cloud samples. The variation of beam filling and sensitivity clip factors with respect to molecular cloud samples is possibly significant and will be investigated in the future.

Due to the uncertainty of beam filling factors, estimations of excitation temperatures and optical depths for small molecular clouds are subject to large errors. This is usually the case for extragalactic observations, in which most molecular clouds are unresolved. At least a factor of 2 should be used to calibrate the brightness temperature in the application of radiative transfer equations.

We estimate beam filling factors of observations toward Giant molecular clouds (GMCs) in size of ~ 50 -100 pc (Motte et al. 2018) and dense cores in size of ~ 0.1 -0.2 pc (Motte et al. 2018) based on Equation 9. As demonstrated in Figure 9, GMC observations with ALMA toward the Local Group galaxies (Sun et al. 2018) have an angular size of 2-3 beam sizes, and the corresponding η is about 0.5. For those observations, the α_{vir} would be overestimated by a factor of 2. For GMCs at a medium distance of ~ 5 kpc in the Milky Way, observations of the CfA 1.2-m (Dame et al. 2001) yield η of ~ 0.75 , and with PMO 13.7-m (Su et al. 2019), the η of GMCs would be approximately 0.9. Seen by PMO 13.7-m, dense cores in a close high-mass star forming region, Orion (~ 400 pc) have an angular size of 1-2 beam sizes, and their η would be about 0.4. Consequently, observations with relatively low angular resolutions would significantly underestimate the brightness temperature.

4.4. Sensitivity clip factors of molecular clouds

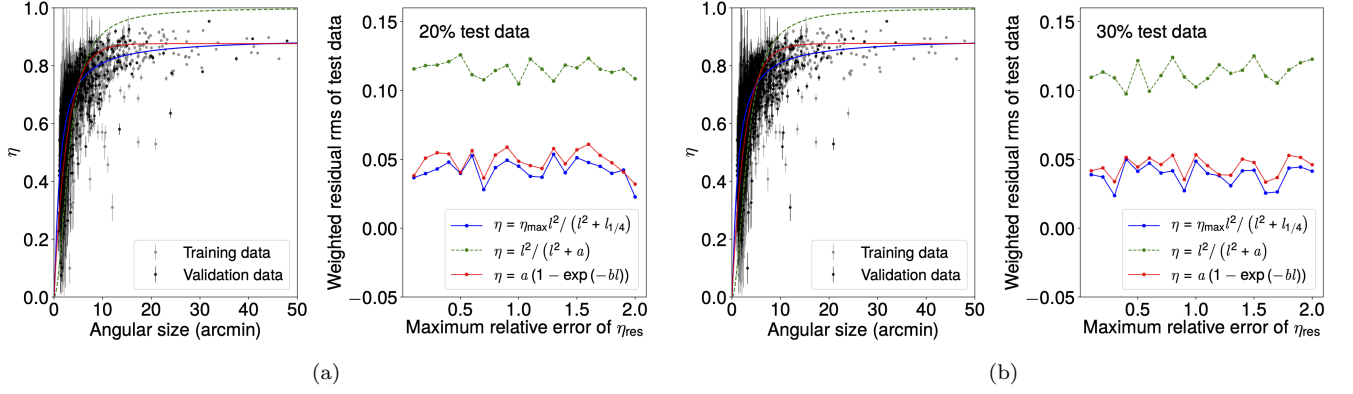


Figure 8. A comparison of three functions to model the relationship of η and the angular size (l). The molecular cloud samples used are ^{12}CO clouds in the Local arm. Panel (a) uses 80% of the samples to fit the model and the rest 20% for testing, while the validation data ratio in panel (b) is 30%. The right side of each panel plots the variation of the weighted rms residual of the validation samples with respect to a maximum relative error threshold for each model. See Equation 8 (blue), 11 (green), and 12 (red) for the form of three models. As examples, on the left side of each panel, we display the training (gray) and validation (black) samples (maximum relative errors less than 0.2), together with the fitting of three models.

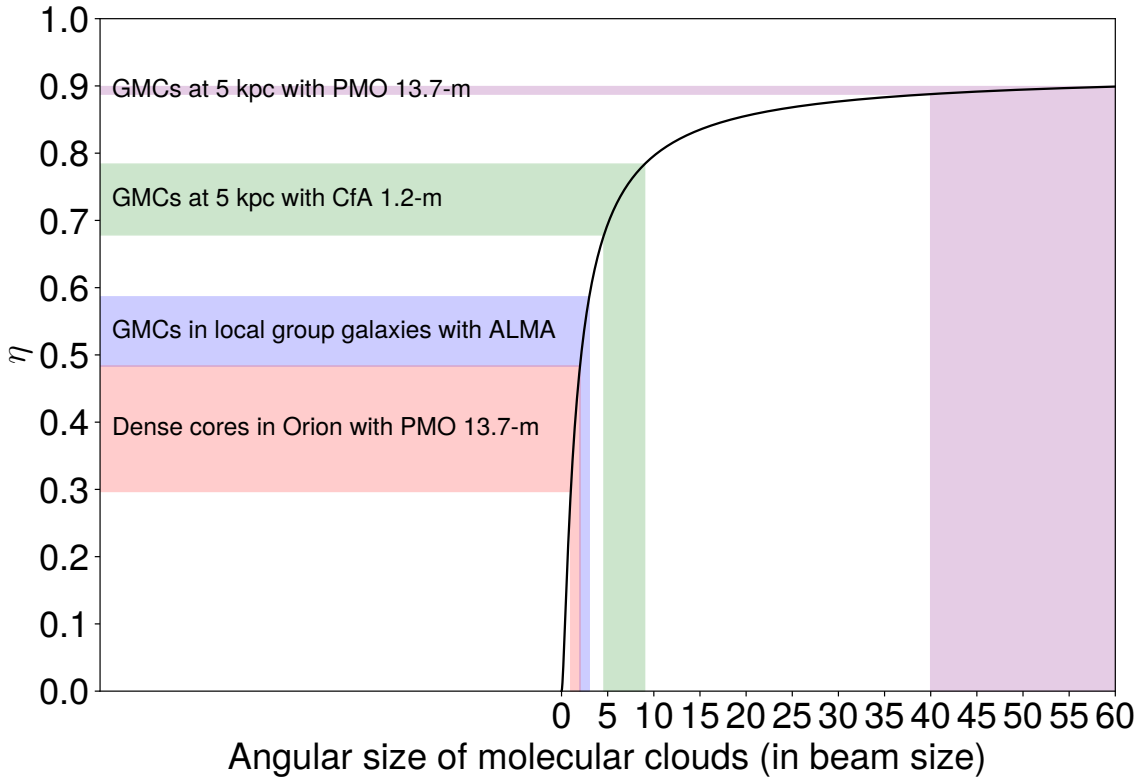


Figure 9. Beam filling factors of molecular clouds in different observational cases. See Equation 9 for the form of the black solid line. We list four typical situations with respect to GMCs (two Galactic cases and an extragalactic one) and dense cores (in Orion).

Results of the sensitivity clip factors reveal that measured flux is incomplete. According to the relationship in Figure 7, the sensitivity clip factor is about 0.5 for a cloud with a mean voxel SNR of 3.3. This suggests that a large fraction of flux is missed for barely detected molecular clouds. Apparently, physical properties of C^{18}O ($J = 1 \rightarrow 0$) are largely uncertain due to their low beam filling and sensitivity clip factors.

Table 5. Observation parameters of four surveys.

Survey Name	Spectral line	Beam size	l	b	V_{LSR}	δv	rms noise	Cloud number
			($^{\circ}$, $^{\circ}$)	($^{\circ}$, $^{\circ}$)	(km s^{-1})	(km s^{-1})	(K)	
CfA 1.2-m ^a	$^{12}\text{CO } (J = 1 \rightarrow 0)$	$8.5''$	[17, 75]	[-3, 4.9]	[-87, 140]	1.3	~ 0.1	243
GRS ^b	$^{13}\text{CO } (J = 1 \rightarrow 0)$	$46''$	[25.8, 49.7]	[-1, 1]	[-5, 70]	0.2	~ 0.1	6721
OGS ^c	$^{12}\text{CO } (J = 1 \rightarrow 0)$	$46''$	[102.5, 141.5]	[-3, 5.4]	[-100, 20]	0.8	~ 0.6	4928
COHRS ^d	$^{12}\text{CO } (J = 3 \rightarrow 2)$	$16''$	[24.75, 48.75]	[-0.275, 0.275]	[-5, 70]	1.0	~ 0.4	11877

(a) Dame et al. (2001). (b) Jackson et al. (2006). (c) Heyer et al. (1998). (d) Dempsey et al. (2013).

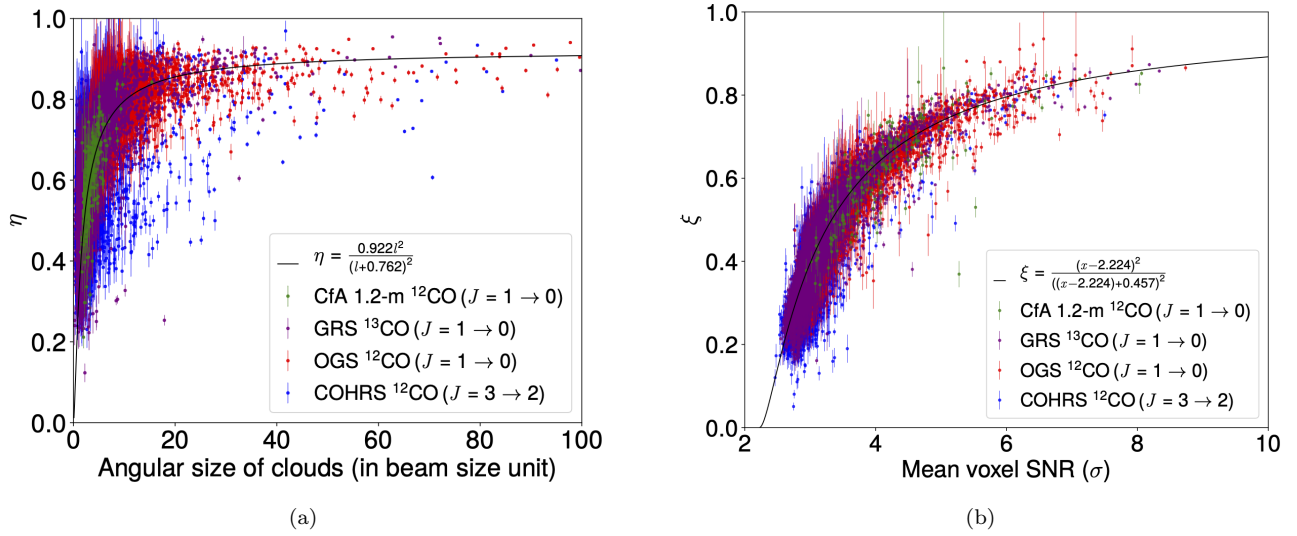


Figure 10. Beam filling and sensitivity clip factors of molecular clouds in four CO surveys (see Table 5). For clarity purposes, molecular clouds with beam filling factor relative errors larger than 20% were removed. As a comparison, we display results derived with the MWISP survey in black solid lines: (a) the η and the angular size relationship (see Equation 9) and (b) the ξ and the mean voxel SNR relationship (see Figure 7).

The sensitivity clip factor is remarkably consistent between molecular clouds. This universality suggests that the brightness temperature distribution of most molecular clouds is similar. As shown in Figure 7, the dispersion of ξ is small, meaning that molecular clouds with the same mean voxel SNR miss a similar fraction of flux, this only happens when their distributions of brightness temperatures are the same.

4.5. Comparison with other surveys

In order to see the variation of beam filling sensitivity clip factors under other observations with different spectral line tracers, beam sizes, and sensitivities, we compare four CO surveys with the MWISP survey. Table 5 lists observational parameters and PPV ranges of four examined surveys, and for the large-scale ^{12}CO survey (Dame et al. 2001) conducted with CfA 1.2-m, we choose a uniformly sampled region that has a large Galactic latitude coverage in the first Galactic quadrant.

With the same smoothing and cloud identification procedure, we calculated η and ξ of molecular clouds for the four CO surveys. As demonstrated in Figure 10, their beam filling and sensitivity clip factors are remarkably consistent with that derived with the MWISP survey. This indicates that despite of having different sensitivities, beam sizes, and even spectral lines, beam filling and sensitivity clip factors of molecular clouds show similar relationships with molecular cloud sizes and mean voxel SNRs.

Our analysis methodology is applicable to other phases of the ISM. Berkhuijsen (1999) studied the volume filling factor of multiple phases of the ISM, including H II, H I, molecular, and dust clouds, and the results suggest similar

structures for ionized and molecular clouds. It is interesting to compare the results with directly measured beam filling and sensitivity clip factors of the ISM, which could possibly reveal the structure and the distribution of the ISM.

5. SUMMARY

We studied beam filling and sensitivity clip factors of molecular clouds by simulating observations with large beam sizes and low sensitivities using the MWISP CO survey in the first Galactic quadrant. The beam filling factor is used to calibrate the brightness temperature, and the sensitivity clip factor is used to estimate the completeness of the flux. The beam filling factor is modeled with a two-component function according to the variation of the mean T_{mb} with respect to beam sizes, while the sensitivity clip factor is modeled using a quadratic function with a fast decreasing tail. In order to examine the collective and individual properties, we derived beam filling and sensitivity clip factors based on both the entire images and molecular cloud samples.

The main results can be summarized as follows:

1. Beam filling factors of ^{12}CO and ^{13}CO are approximately unity in the Local (~ 1 kpc), the Sagittarius (~ 3 kpc), and the Scutum (~ 6 kpc) arm, but drops to ~ 0.7 and ~ 0.6 in the Outer arm (~ 15 kpc), respectively. C^{18}O however, decreases significantly with distance, and is approximately zero in the Outer arm. The sensitivity clip factor shows similar variations with the beam filling factors, but is systematically lower by ~ 0.2 .
2. The beam filling factor is mainly correlated with the angular size l in the beam size unit and can be approximated with $0.922l^2 / (l + 0.762)^2$. The average beam filling factors of molecular clouds identified with DBSCAN can be derived using this correlation.
3. We derived a relationship between the observed flux and the mean voxel SNR (x), and the ratio of the observed flux to the total flux is approximately $(x - 2.224)^2 / (x - 2.224 + 0.457)^2$. This relationship can be used to estimate the total flux.
4. The η -size and ξ -sensitivity relationships seem to be universal suggested by the comparison with other existing CO surveys.

ACKNOWLEDGMENTS

We would like to show our gratitude to support members of the MWISP group, Xin Zhou, Zhiwei Chen, Shaobo Zhang, Min Wang, Jixian Sun, and Dengrong Lu, and observation assistants at PMO Qinghai station for their long-term observation efforts. We are also immensely grateful to other member of the MWISP group, Ye Xu, Hongchi Wang, Zhibo Jiang, Xuepeng Chen, Yiping Ao for their useful discussions. This work was sponsored by the Ministry of Science and Technology (MOST) Grant No. 2017YFA0402701, Key Research Program of Frontier Sciences (CAS) Grant No. QYZDJ-SSW-SLH047, National Natural Science Foundation of China Grant No. 11773077, U1831136, and 12003071, and the Youth Innovation Promotion Association, CAS (2018355).

Facilities: PMO 13.7-m

Software: astropy (Astropy Collaboration et al. 2013), SciPy

REFERENCES

- | | |
|---|---|
| <p>Acharyya, A., Krumholz, M. R., Federrath, C., et al. 2020, MNRAS, 495, 3819, doi: 10.1093/mnras/staa1100</p> <p>André, P., Men'shchikov, A., Bontemps, S., et al. 2010, A&A, 518, L102, doi: 10.1051/0004-6361/201014666</p> <p>Astropy Collaboration, Robitaille, T. P., Tollerud, E. J., et al. 2013, A&A, 558, A33, doi: 10.1051/0004-6361/201322068</p> | <p>Bally, J., Langer, W. D., Stark, A. A., & Wilson, R. W. 1987, ApJL, 312, L45, doi: 10.1086/184817</p> <p>Berkhuijsen, E. M. 1999, in Plasma Turbulence and Energetic Particles in Astrophysics, ed. M. Ostrowski & R. Schlickeiser, 61–65</p> <p>Burton, M. G., Hollenbach, D. J., & Tielens, A. G. G. M. 1990, ApJ, 365, 620, doi: 10.1086/169516</p> |
|---|---|

- Dame, T. M., Hartmann, D., & Thaddeus, P. 2001, *ApJ*, 547, 792, doi: [10.1086/318388](https://doi.org/10.1086/318388)
- Dassa-Terrier, J., Melchior, A.-L., & Combes, F. 2019, *A&A*, 625, A148, doi: [10.1051/0004-6361/201834069](https://doi.org/10.1051/0004-6361/201834069)
- Dempsey, J. T., Thomas, H. S., & Currie, M. J. 2013, *ApJS*, 209, 8, doi: [10.1088/0067-0049/209/1/8](https://doi.org/10.1088/0067-0049/209/1/8)
- Falgarone, E., Phillips, T. G., & Walker, C. K. 1991, *ApJ*, 378, 186, doi: [10.1086/170419](https://doi.org/10.1086/170419)
- Flower, D. R., Pineau des Forêts, G., & Rabli, D. 2010, *MNRAS*, 409, 29, doi: [10.1111/j.1365-2966.2010.17501.x](https://doi.org/10.1111/j.1365-2966.2010.17501.x)
- Gong, M., Ostriker, E. C., & Kim, C.-G. 2018, *ApJ*, 858, 16, doi: [10.3847/1538-4357/aab9af](https://doi.org/10.3847/1538-4357/aab9af)
- Heiles, C., & Troland, T. H. 2003, *ApJ*, 586, 1067, doi: [10.1086/367828](https://doi.org/10.1086/367828)
- Heyer, M., & Dame, T. M. 2015, *ARA&A*, 53, 583, doi: [10.1146/annurev-astro-082214-122324](https://doi.org/10.1146/annurev-astro-082214-122324)
- Heyer, M. H., Brunt, C., Snell, R. L., et al. 1998, *ApJS*, 115, 241, doi: [10.1086/313086](https://doi.org/10.1086/313086)
- Jackson, J. M., Rathborne, J. M., Shah, R. Y., et al. 2006, *ApJS*, 163, 145, doi: [10.1086/500091](https://doi.org/10.1086/500091)
- Leroy, A. K., Usero, A., Schrubba, A., et al. 2017, *ApJ*, 835, 217, doi: [10.3847/1538-4357/835/2/217](https://doi.org/10.3847/1538-4357/835/2/217)
- Mangum, J. G., & Shirley, Y. L. 2015, *PASP*, 127, 266, doi: [10.1086/680323](https://doi.org/10.1086/680323)
- Mathis, J. S., Mezger, P. G., & Panagia, N. 1983, *A&A*, 500, 259
- Melchior, A.-L., & Combes, F. 2016, *A&A*, 585, A44, doi: [10.1051/0004-6361/201526257](https://doi.org/10.1051/0004-6361/201526257)
- Molinari, S., Swinyard, B., Bally, J., et al. 2010, *A&A*, 518, L100, doi: [10.1051/0004-6361/201014659](https://doi.org/10.1051/0004-6361/201014659)
- Motte, F., Bontemps, S., & Louvet, F. 2018, *ARA&A*, 56, 41, doi: [10.1146/annurev-astro-091916-055235](https://doi.org/10.1146/annurev-astro-091916-055235)
- Norman, C., & Silk, J. 1980, *ApJ*, 238, 158, doi: [10.1086/157969](https://doi.org/10.1086/157969)
- Pineda, J. L., Mizuno, N., Stutzki, J., et al. 2008, *A&A*, 482, 197, doi: [10.1051/0004-6361:20078769](https://doi.org/10.1051/0004-6361:20078769)
- Reid, M. J., Dame, T. M., Menten, K. M., & Brunthaler, A. 2016, *ApJ*, 823, 77, doi: [10.3847/0004-637X/823/2/77](https://doi.org/10.3847/0004-637X/823/2/77)
- Reid, M. J., Menten, K. M., Brunthaler, A., et al. 2014, *ApJ*, 783, 130, doi: [10.1088/0004-637X/783/2/130](https://doi.org/10.1088/0004-637X/783/2/130)
- Rosolowsky, E., & Leroy, A. 2006, *PASP*, 118, 590, doi: [10.1086/502982](https://doi.org/10.1086/502982)
- Stanimirovic, S., Staveley-Smith, L., Dickey, J. M., Sault, R. J., & Snowden, S. L. 1999, *MNRAS*, 302, 417, doi: [10.1046/j.1365-8711.1999.02013.x](https://doi.org/10.1046/j.1365-8711.1999.02013.x)
- Stutzki, J., Bensch, F., Heithausen, A., Ossenkopf, V., & Zielinsky, M. 1998, *A&A*, 336, 697
- Su, Y., Yang, J., Zhang, S., et al. 2019, *ApJS*, 240, 9, doi: [10.3847/1538-4365/aaf1c8](https://doi.org/10.3847/1538-4365/aaf1c8)
- Sun, J., Leroy, A. K., Schrubba, A., et al. 2018, *ApJ*, 860, 172, doi: [10.3847/1538-4357/aac326](https://doi.org/10.3847/1538-4357/aac326)
- Yan, Q.-Z., Yang, J., Su, Y., Sun, Y., & Wang, C. 2020, *ApJ*, 898, 80, doi: [10.3847/1538-4357/ab9f9c](https://doi.org/10.3847/1538-4357/ab9f9c)
- Yan, Q.-Z., Yang, J., Sun, Y., Su, Y., & Xu, Y. 2019, *ApJ*, 885, 19, doi: [10.3847/1538-4357/ab458e](https://doi.org/10.3847/1538-4357/ab458e)